

# Assessment of Forest Aboveground Biomass Stocks and Dynamics with Inventory Data, Remotely Sensed Imagery and Geostatistics

Helder Viana<sup>1</sup>, Domingos Lopes<sup>2</sup> and José Aranha<sup>2</sup>

<sup>1</sup>*Polytechnic Institute of Viseu*

<sup>2</sup>*CITAB - University of Trás-os-Montes e Alto Douro  
Portugal*

## 1. Introduction

Several issues, related with forest fires, forest disturbances (García-Martín et al., 2008), forest productivity (Chirici et al., 2007; Palmer et al., 2009), forest changes over time (Hu & Wang, 2008), or the role of forests in the global carbon balance cycle (Hese et al., 2005) are, nowadays, the focus of numerous studies and investigations. All these subjects demand the knowledge about aboveground biomass (AGB) stocks and/or its dynamics. Besides the availability of biomass, the information about the growth of forests is of increasing importance. This variable, which is related with the total biomass growth in a specific ecosystem, is called Net Primary Production (NPP). Annual NPP represents the net amount of carbon captured by plants through photosynthesis each year (Melillo et al., 1993; Cao & Woodward, 1998). In practice, NPP can be defined and measured in terms of either biomass or CO<sub>2</sub> exchange (Field et al., 1995). Waring et al. (1998) define NPP as the sum of live biomass periodic increment ( $\Delta B$ ) and dead biomass (losses, e.g. broken branches, fallen leaves) [ $NPP = \Delta B + \text{losses}$ ]. NPP is an important ecological variable due to its relevance for accurate ecosystem management and for monitoring the impact of human activity on ecosystems vegetation at a range of spatial scales: local, regional and global (Melillo et al., 1993). It is one of the most complete and complex variables, since it reflects the growth of the entire ecosystem thus avoiding the analysis of only part of its components. NPP provides a complete view of the ecosystem including information, not only from the arboreal stratum, but also from the shrubs and all the litter produced from each stratum. Thus, the significance of NPP not only reflects the complexity of its measurement or estimation, but also its integrative ecological perspective ecosystems.

Mapping AGB stocks or NPP with the utmost accuracy and expedite methodologies is therefore a challenge. The need of continuous maps where the phenomenon under study can be individually analysed or used as auxiliary variable in a specific model requires that the spatial predictions are represented in the most accurate way. Over the years different spatial prediction methods have been explored in diverse data type (Isaaks & Srivastava, 1989; Goovaerts, 1997; Labrecque et al., 2006; Sales et al., 2007; Meng et al., 2009). Some approaches have a simple application methodology however others are sometimes complex in what concerns to their implementation, or the selection of the variables to be used.

Estimation of AGB has been made by a range of methods, from field measurements to remote sensing-based methods, as well GIS-based modelling approaches with auxiliary data (Lu, 2006). Traditionally, to predict the spatial distribution of AGB throughout the territory, the variables calculated based on the forest inventory dataset were usually assigned to the forest polygons, stratified by species, and mapped by aerial photos interpretation. Despite the field measurements being the most accurate methods for collecting biomass data, the level of precision of the resultant biomass map will depend of the land cover classification detail and of the sample intensity. In fact, the forest inventories data at regional or national scale are often not spatially exhaustive enough to generate continuous AGB estimates, thus limiting the use of this approach over large areas. An additional limitation is the long temporal resolution of these estimations, generally made in cycles of 10 or more years, which could not be compatible with the need of analysis and monitoring of the ecosystems' dynamics.

Remote sensing-based methods have been the most widely used approach to map AGB. The utility of the spectral information recorded by remote sensing for monitoring vegetation or gathering ecophysiological information over large areas is very well recognized, since satellite data became accessible for land cover dynamic studies. Different imagery data have been employed, such as coarse spatial-resolution data as SPOT-VEGETATION (Chirici et al., 2007; Jarlan et al., 2008), NOAA AVHRR (Häme et al., 1997; Atkinson et al., 2000), MODIS (Zheng et al., 2007, Muukkonen & Heiskanen, 2007); medium spatial-resolution data as ASTER (Muukkonen & Heiskanen, 2007), Landsat TM/ETM+ (Tomppo et al., 2002; Rahman et al., 2005; Meng et al., 2009); high spatial-resolution data as IRS P6 LISS-IV (Madugundu et al., 2008) and radar data (Hyde et al., 2007; Liao et al., 2009).

AGB can be estimated by means of Direct Radiometric Relationships (DRR), which consist in establishing regression relationships, such as ordinary least squares (OLS), between the satellite spectral data (e.g. individual spectral bands, band ratios, vegetation indices and other possible transformations) as independent variables, and the measured parameter at each corresponding inventory sample plot position in each forest cover strata. AGB can be directly predicted by multiple regression analysis between spectral data response and biomass amount (Labrecque et al., 2006; Muukkonen & Heiskanen, 2007); by nonparametric approaches including K nearest neighbour (KNN) (Tomppo, 1991; Meng et al., 2007), or by artificial neural network (ANN) (Liao et al., 2009); or indirectly predicted by using characteristic such as crown diameter or leaf area index (LAI). In this case, these variables are firstly derived from the imagery data and subsequently used in regression analysis to estimate AGB.

Spatial prediction models (algorithms) have been used for spatially predicting vegetation attributes. In general, these interpolation techniques are classified in deterministic and statistical (probabilistic) models (Isaaks & Srivastava, 1989; Goovaerts, 1997; Hengl, 2009). Attending that in the Earth sciences there is usually a lack of sufficient knowledge concerning how properties vary in space, a deterministic model may not be appropriate. Therefore, to make predictions at locations for which observations do not exist, with inherent uncertainty in predictions, the use of probabilistic models is necessary (Lloyd, 2007).

Spatial statistics and geostatistics were developed to describe and analyze the variation in both natural and man-made phenomena on above or below the land surface (Cressie, 1993). Largely developed by Matheron (1963) in the 1960s, to evaluate recoverable reserves for the mining industry, geostatistical models have been systematically applied in a wide range of fields (Cressie, 1993; Goovaerts, 1997). Today, geostatistics and the theory of regionalized variables (Matheron, 1971) are used to explore and describe the presence of spatial variation that occur in most natural resource variables. Introduced to remote sensing by Woodcock et al. (1988) and by Curran (1988), geostatistical models have been used to design optimum sampling

schemes for image data and ground data; to increase the accuracy in which remotely sensed data can be used to classify land cover; or to estimate continuous variables. Geostatistical models are reported in numerous textbooks (e.g. Isaaks & Srivastava, 1989; Cressie 1993; Goovaerts, 1997; Deutsch & Journel, 1998; Webster & Oliver, 2007; Hengl, 2009; Sen, 2009) such as Kriging (plain geostatistics); environmental correlation (e.g. regression-based); Bayesian-based models (e.g. Bayesian Maximum Entropy) and hybrid models (e.g. regression-kriging). Despite Regression-kriging (RK) is being implemented in several fields, as soil science, few studies explored this approach to spatially predict AGB with remotely sensed data as auxiliary predictor. Hence, this research makes use of RK and remote sensing data to analyse if spatial AGB predictions could be improved.

This research presents two case studies in order to explore the techniques of remote sensing and geostatistics for mapping the AGB and NPP. The first, aims to compare three approaches to estimate *Pinus pinaster* AGB, by means of remotely sensed imagery, field inventory data and geostatistical modeling. The second aims to analyse if NPP of *Eucalyptus globulus* and *Pinus pinaster* species can easily and accurately be estimated using remotely sensed data.

## 2. Case study I – Aboveground biomass prediction by means of remotely sensed imagery, field inventory data and geostatistical modeling

### 2.1 Study area

This study was carry out in Portugal (Continental), extending from the latitudes of 36° 57' 23" and 42° 09' 15"N and the longitudes of 09° 30' 40" and 06° 10' 45" W (Figure 1). This area

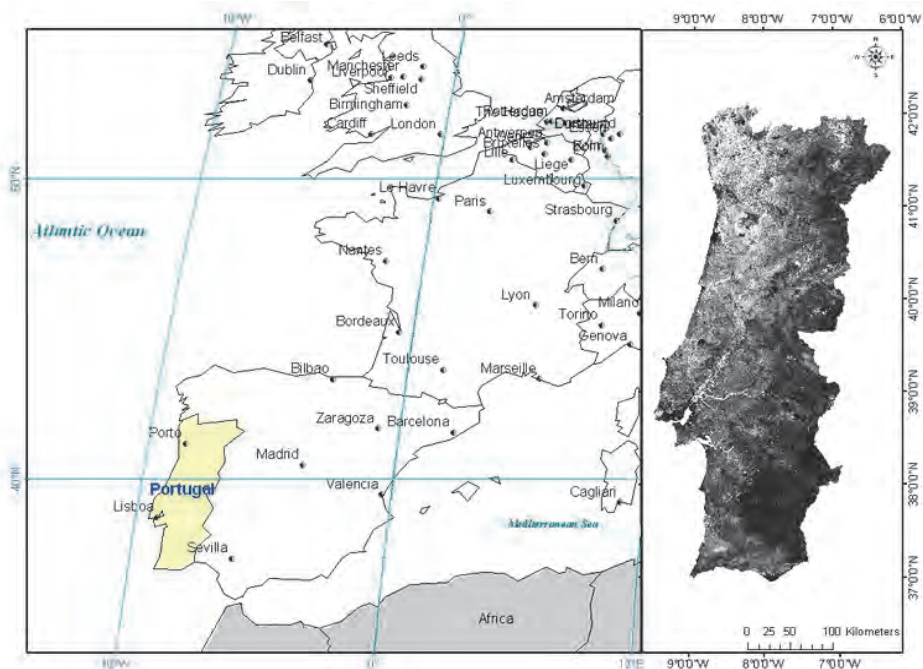


Fig. 1. Study area location

includes two distinctive bioclimatic regions: a Mediterranean bioclimate in everywhere except a small area in the North with a temperate bioclimate. With four distinct weather seasons, the average annual temperatures range from about 7 °C in the highlands of the interior north and center and about 18 °C in the south coast. Average annual precipitation is more than 3000 mm at the north and less than 600 mm at the south.

Due to a 20 years of severe wild fires during summer time, and intense people movement from rural areas to sea side cities or county capital, forestry landscape changed from large trees' stands interspersed by agricultural lands, to a fragmented landscape. The land cover is fragmented with small amount of suitable soils for agriculture and the main areas occupied by forest spaces. Forest activity is a direct source of income for a vast forest products industry, which employs a significant part of the population.

## **2.2 Methods and data**

### **2.2.1 GIS and field data**

In a first stage a GIS project (ArcGis 9.x), was created in order to identify *Pinus pinaster* pure stands, over a Portuguese Corine Land Cover Map (CLC06, IGP, 2010). In a second stage, GIS project database was updated with the dendrometric data collected during Portuguese National Forestry Inventory (AFN, 2006), in order to derive AGB allometric equations, with Vegetation Indices values as independent variable. A total of 328 field plots of pure pine stands were used. The inventory dataset was further used in spatial prediction analysis, to create continuous AGB maps for the study area.

### **2.2.2 Biomass estimation from the forest inventory dataset**

In order to calculate the biomass exclusively from the forest inventory, the biomass values measured in each field plot were spatially assigned to the pine stands land cover map polygons. In the cases where multiple plots were coincident with the same polygon, weighted averages were calculated proportionally to the area of occupation in that polygon.

### **2.2.3 Remote sensing imagery**

In this research we used the Global MODIS vegetation indices dataset (h17v04 and h17v05) from the Moderate Resolution Imaging Spectroradiometer (MODIS) from 29 August 2006: (MOD13Q1.A2006241.h17v04.005.2008105184154.hdf; and MOD13Q1.A2006241.h17v05.005.2008105154543.hdf), freely available from the US Geological Survey (USGS) Earth Resources Observation and Science (EROS) Center. The Global MOD13Q1 data includes the MODIS Normalized Difference Vegetation Index (NDVI) and a new Enhanced Vegetation Index (EVI) provided every 16 days at 250-meter spatial resolution as a gridded level-3 product in the Sinusoidal projection.

([https://lpdaac.usgs.gov/lpdaac/products/modis\\_products\\_table/vegetation\\_indices/16\\_day\\_l3\\_global\\_250m/mod13q1](https://lpdaac.usgs.gov/lpdaac/products/modis_products_table/vegetation_indices/16_day_l3_global_250m/mod13q1)).

MODIS data was projected to the same Portuguese coordinate system (Hayford-Gauss, Datum of Lisbon with false origin) used in the GIS project.

### **2.2.4 Direct Radiometric Relationships (DRR)**

Using GIS tools, field inventory dataset was updated with information from MODIS images. The spectral information extracted (NDVI and EVI) was then used as independent variables for developing regression models. Linear, logarithmic, exponential, power,

and second-order polynomial functions were tested on data relationship analysis. The best model achieved was then applied to the imagery data, and the predicted aboveground biomass map was produced. In some pixels where Vegetation index values were very low, the biomass values predicted by the regression equations were negative, so these pixels were removed, because in reality negative biomass values are not possible.

**2.2.5 Geostatistical modeling**

Regression-kriging (RK) (Odeh et al., 1994, 1995) is a hybrid method that involves either a simple or multiple-linear regression model (or a variant of the generalized linear model and regression trees) between the target variable and ancillary variables, calculating residuals of the regression, and combining them with kriging. Different types or variant of this process, but with similar procedures, can be found in literature (Ahmed & De Marsily, 1987; Knotters et al.; 1995; Goovaerts; 1999; Hengl et al.; 2004, 2007), which can cause confusion in the computational process.

In the process of RK the predictions ( $\hat{z}_{rk}(s_0)$ ) are combined from two parts; one is the estimate  $\hat{m}(s_0)$  obtained by regressing the primary variable on the  $k$  auxiliary variables  $q_k(s_0)$  and  $q_0(s_0) = 1$ ; the second part is the residual estimated from kriging ( $\hat{e}(s_0)$ ). RK is estimated as follows (Eqs. 1 and 2):

$$\hat{z}_{rk}(s_0) = \hat{m}(s_0) + \hat{e}(s_0) \tag{1}$$

$$\hat{z}_{rk}(s_0) = \sum_{k=0}^v \hat{\beta}_k \cdot q_k(s_0) + \sum_{i=1}^n w_i(s_0) \cdot e(s_i) \tag{2}$$

where  $\hat{\beta}_k$  are estimated drift model coefficients ( $\hat{\beta}_0$  is the estimated intercept), optimally estimated from the sample by some fitting method, e.g. ordinary least squares (OLS) or, optimally, using generalized least squares (GLS), to take the spatial correlation between individual observations into account (Cressie, 1993);  $w_i$  are kriging weights determined by the spatial dependence structure of the residual and  $e(s_i)$  are the regression residuals at location  $s_i$ . RK was performed using the GSTAT package in IDRISI software (Eastman, 2006) both to automatically fit the variograms of residuals and to produce final predictions (Pebesma, 2001 and 2004). The first stage of geostatistical modeling consists in computing the experimental variograms, or semivariogram, using the classical formula (Eq. 3):

$$\hat{\gamma}(h) = \frac{1}{2N(h)} \sum_{i=1}^{N(h)} [z(x_i) - z(x_i + h)]^2 \tag{3}$$

where  $\hat{\gamma}(h)$  is the semivariance for distance  $h$ ,  $N(h)$  the number of pairs for a certain distance and direction of  $h$  units, while  $z(x_i)$  and  $Z(x_i + h)$  are measurements at locations  $x_i$  and  $x_i + h$ , respectively.

Semivariogram gives a measure of spatial correlation of the attribute in analysis. The semivariogram is a discrete function of variogram values at all considered lags (e.g. Curran 1988; Isaaks & Srivastava 1989). Typically, the semivariance values exhibit an ascending

behaviour near the origin of the variogram and they usually level off at larger distances (the sill of the variogram). The semivariance value at distances close to zero is called the nugget effect. The distance at which the semivariance levels off is the range of the variogram and represents the separation distance at which two samples can be considered to be spatially independent.

For fitting the experimental variograms we tested the exponential, the gaussian and the spherical models, using iterative reweighted least squares estimation (WLS, Cressie, 1993). Finally, RK was carried out according to the methodology described in <http://spatial-analyst.net>. The EVI image was used as predictor (auxiliary map) in RK. GSTAT produces the predictions and variance map, which is the estimate of the uncertainty of the prediction model, i.e. precision of prediction.

### 2.2.6 Validation of the predicted maps

The validation and comparison of the predicted AGB maps were made by examining the discrepancies between the known data and the predicted data. The dataset was, prior to estimates, divided randomly into two sets: the prediction set (276 plots) and the validation set (52 plots). According to Webster & Oliver (1992), to estimate a variogram 225 observations are usually reliable. The prediction approaches were evaluated by comparing the basic statistics of predicted AGB maps (e.g., mean and standard deviation) and the difference between the known data and the predicted data were examined using the mean error, or bias mean error (ME), the mean absolute error (MAE), standard deviation (SD) and the root mean squared error (RMSE), which measures the accuracy of predictions, as described in Eqs. (4-7).

$$SD = \sqrt{\frac{1}{N-1} \sum_{i=1}^N (e_i - \bar{e})^2} \quad (4)$$

$$ME = \frac{1}{N} \sum_{i=1}^N (\hat{e}_i - e_i) \quad (5)$$

$$MAE = \frac{1}{N} \sum_{i=1}^N |\hat{e}_i - e_i| \quad (6)$$

$$RMSE = \sqrt{\frac{1}{N} \sum_{i=1}^N (\hat{e}_i - e_i)^2} \quad (7)$$

where:  $N$  is the number of values in the dataset,  $\hat{e}_i$  is the estimated biomass,  $e_i$  is the biomass values measured on the validation plots and  $\bar{e}$  is the mean of biomass values of the sample.

## 2.3 Results and discussion

### 2.3.1 *Pinus pinaster* stands characteristics

The descriptive statistics of pine stands data are presented in Table 1, where:  $N$  is the number of trees;  $t$  is the forestry stand age;  $h_{dom}$  is the dominant height;  $dbh_{dom}$  is the dominant diameter at breast height;  $SI$  is the site index;  $BA$  is the basal area;  $V$  is the stand volume and  $AGB$  is the biomass in the sample plot.

The pine stands are highly heterogeneous with ages ranging from 8 to 110 years old and the biomass per hectare ranging from 0.9 to 136.1 ton ha<sup>-1</sup>. The values of Biomass present a normal distribution with mean  $m = 52.12$  ton ha<sup>-1</sup> and standard deviation  $\sigma = 32.32$  ton ha<sup>-1</sup> (Figure 2).

| Pine stands plots |                           |        |                  |                    |      |                                    |                                    |                         |
|-------------------|---------------------------|--------|------------------|--------------------|------|------------------------------------|------------------------------------|-------------------------|
|                   | N                         | t      | h <sub>dom</sub> | dbh <sub>dom</sub> | SI   | BA                                 | V                                  | AGB                     |
|                   | (trees ha <sup>-1</sup> ) | (year) | (m)              | (cm)               | (m)  | (m <sup>2</sup> ha <sup>-1</sup> ) | (m <sup>3</sup> ha <sup>-1</sup> ) | (ton ha <sup>-1</sup> ) |
| Mean              | 566                       | 31     | 13.4             | 25.3               | 11.8 | 14.39                              | 99.46                              | 52.12                   |
| Min               | 20                        | 8      | 4.6              | 8.9                | 0.0  | 0.41                               | 1.37                               | 0.85                    |
| Max               | 2219                      | 110    | 36.5             | 59.0               | 69.0 | 38.34                              | 259.03                             | 136.09                  |
| SD                | 405.2                     | 15.9   | 4.0              | 8.0                | 11.5 | 7.64                               | 61.86                              | 32.32                   |

Table 1. Descriptive statistics of data measured in the forest inventory dataset

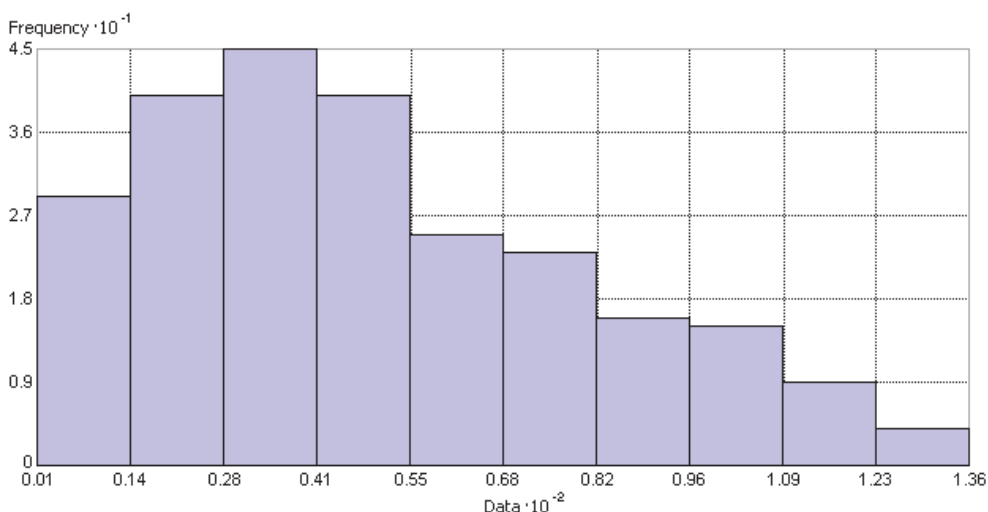


Fig. 2. Histogram of the distribution of the AGB (ton ha<sup>-1</sup>) in the forest inventory dataset

### 2.3.2 Aboveground biomass estimation from the inventory dataset

The estimates based in the inventory dataset were achieved by assigning the 328 field plot biomass values (weighted by each polygon area) into all the polygons of the pine cover class. After the global calculation, the dataset used for training (276 plots) was used to make a first validation of this approach. Hence, a regression was established between the biomass values, measured in the field plots, and the forest inventory polygon data. In Figure 3 it is presented the positive relationship between the measured and the predicted data with a coefficient of determination ( $R^2$ ) of 0.71.

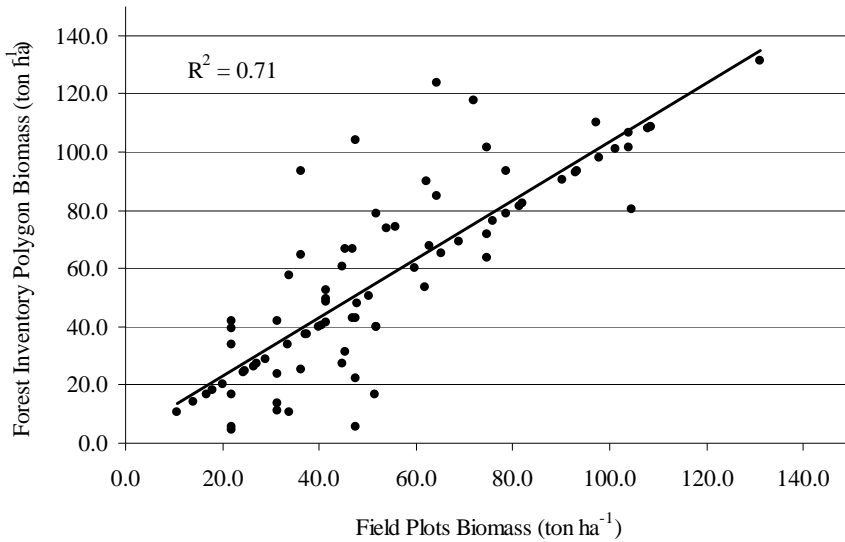


Fig. 3. Relationship between the biomass data measured in field plots and the predicted data extracted in the polygons of land cover map

### 2.3.3 Aboveground biomass estimation from DRR

After performing correlation analyses, between AGB and Vegetation indices, several regression models were developed using stand-wise forest inventory data and the MODIS vegetation indices (NDVI and EVI) as predictors.

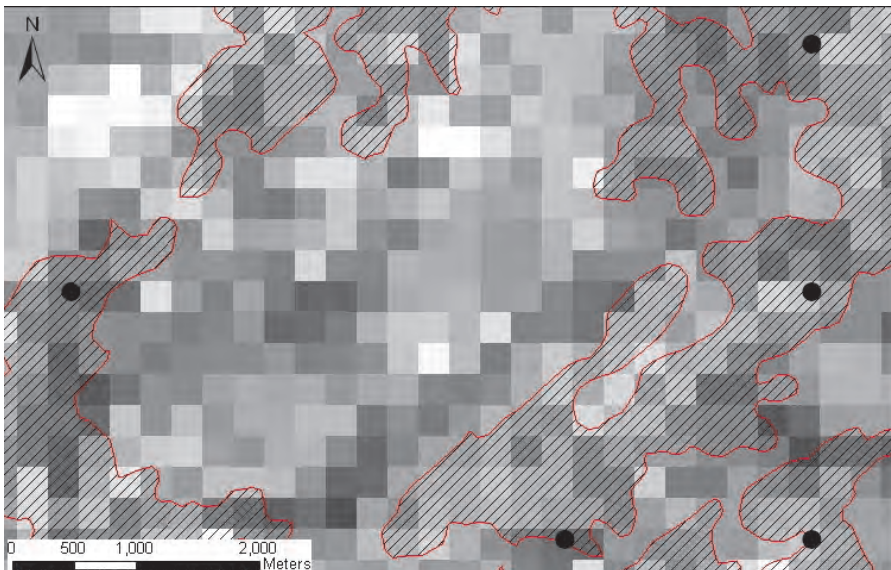


Fig. 4. MODIS image showing the effect of pixels (250m) in the edge of polygons

The best correlation was obtained with EVI as independent variable as (Eq. 8):

$$AGB = 322.4(EVI) - 39.933 \quad (R^2 = 0.32) \quad (8)$$

The AGB was then estimated for the entire study area. The low correlation achieved is explained, in part, by the heterogeneity of pine stands and the high effect of mixed pixels (Burscu et al., 2001) in coarse resolution MODIS data (250 m).

As it can be seen in Figure 4, the reflectance value recorded in the boundary pixels of the polygons limits is not pure, they record both pine stands, and the neighbouring land cover classes reflectance values.

### 2.3.4 Aboveground biomass estimation from geostatistical methods

To spatially estimate the AGB by geostatistical approach, the first step consisted in the modeling and analysis of the experimental semivariograms (Eq. 3). The directional semivariograms of the residuals showed anisotropy at  $38.6^\circ$ , so at this direction were fitted Exponential, Gaussian and Spherical models. Based on experimentation, the exponential variogram model was fitted better (nugget of 703.75 and a partial sill of 390.17 reaching its limiting value at the range of 43,9Km) to the calculated biomass pine stands data (Figure 5). The present data showed a low spatial autocorrelation. The high nugget effect, visible in the figure, which under ideal circumstances should be zero, suggests that there is a significant amount of measurement error present in the data, possibly due to the short scale variation.

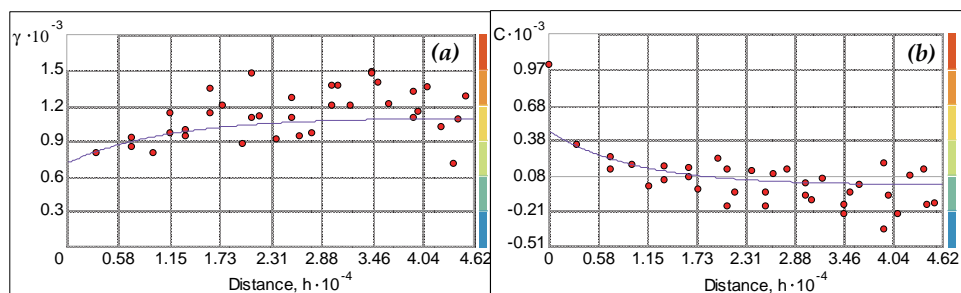


Fig. 5. Directional experimental semivariogram ( $38.6^\circ$ ) with the exponential model fitted (a) and covariance (b)

### 2.3.5 Validation and comparison of the aboveground biomass estimation approaches

The validation of the AGB estimation approaches was made by comparing the calculated basic statistics (Table 2) in the 52 validation random samples. Training and validation sets were compared, by means of a Student's *t* test ( $t = 0.882$  ns), in order to check if they provided unbiased sub-sets of the original data.

As expected, the Inventory Polygons method produced the best statistics. The mean error (ME), which should ideally be zero if the prediction is unbiased, shows a bias in the three approaches, being lower in the Inventory polygons method, and higher in the DRR method. The analysis of the root mean squared errors (RMSE), shows that Inventory Polygons present the lower discrepancies in the estimations (RMSE=33.53%), and RK achieve estimations under lower errors (RMSE=51.95%) than the DRR approach (RMSE=61.62%). Despite this, the errors from the two prediction approaches are very high, which can be

explained by the low correlation found between the vegetation indices data, as explained above. This limitation can be overcome by using remote sensing data with higher spatial resolution. Moreover, the work area must also be sectioned into smaller areas, to minimize the heterogeneity that is observed in very large landscapes.

| Method             | Estimated AGB<br>(average - ton ha <sup>-1</sup> ) | ME<br>(ton ha <sup>-1</sup> ) | MAE<br>(ton ha <sup>-1</sup> ) | RMSE<br>(ton ha <sup>-1</sup> ) | SD<br>(ton ha <sup>-1</sup> ) | RMSE<br>% |
|--------------------|--|-------------------------------|--------------------------------|---------------------------------|-------------------------------|-----------|
| Inventory Polygons | 53.94  | -3.11                         | 11.26                          | 18.09                           | 27.70                         | 33.53     |
| DRR                | 50.23  | -6.83                         | 25.84                          | 30.95                           | 22.03                         | 61.62     |
| RK                 | 52.01  | -5.05                         | 22.70                          | 27.02                           | 19.67                         | 51.95     |

Table 2. Statistics of validation plots for the AGB prediction methods

In order to determine the significance of the differences between interpolation methods, analysis of variance (ANOVA) was performed (Table 3). The results show that, at alpha level 0.05, do not exist significant differences between the biomass values, predicted by the different methods.

| Source  | DF  | SS        | MS      | F     | P     |
|---------|-----|-----------|---------|-------|-------|
| Between | 2   | 122.86    | 61.432  | 0.123 | 0.884 |
| Within  | 243 | 113453.67 | 497.604 |       |       |
| Total   | 245 | 113576.54 |         |       |       |

Table 3. Results from ANOVA to compare the differences between the means of the different prediction methods

A quantitative comparison of the complete AGB maps, estimated by the three approaches, was additionally made. The estimates (ton ha<sup>-1</sup>) are shown in the Table 4. In order to better preserve the land cover areas, the maps were brought to the resolution of 50x50m, and then clipped by the pine land cover mask.

| Method             | Pixels  | Area (ha) | AGB<br>(average - ton ha <sup>-1</sup> ) | Std<br>(ton ha <sup>-1</sup> ) | B (tonnes) |
|--------------------|---------|-----------|--|--------------------------------|------------|
| Inventory Polygons |         | 300446    | 53.8                                     | 30.8                           | 15564351   |
| DRR                | 1191597 | 297899    | 53.8                                     | 20.0                           | 16020055   |
| RK                 | 1189213 | 297303    | 52.8                                     | 21.3                           | 15711245   |

Table 4. Summary statistics of predicted pine AGB maps

The three AGB maps originates very similar average values (ton ha<sup>-1</sup>), and the differences between the maximum and minimum values of total biomass (tonnes) estimated by the different methods varies less than 1.6%.

Although there has been a low discrepancy between the total biomass values, estimated by three maps, the analysis of the correlation coefficient of regressions, carried out between the three maps, show low to moderate correlation between *Inventory Polygons* x *DRR* and *Inventory Polygons* x *RK* methods ( $R = 0.27$  and  $0.40$ , respectively). Only *DRR* x *RK* methods present high correlation values ( $R = 0.95$ ) indicating a very similar biomass estimation at individual pixels (Figure 6).

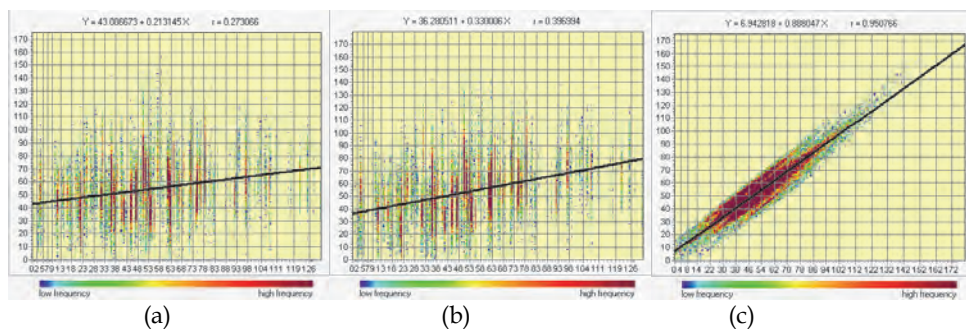


Fig. 6. Regression performed between AGB maps (a) *Inventory Polygons x DRR*; (b) *Inventory Polygons x RK*; (c) *DRR x RK*

Based in the calculated statistics of the validation dataset and in the global biomass estimations for entire area, we can consider that the Regression-kriging geostatistical prediction approach, with remotely sensed imagery as auxiliary variable, increases the classifications accuracy when compared with estimates based merely in the Direct Radiometric Relationships (DRR). Furthermore, the accuracy of these estimations could increase by using imagery data with higher spatial resolution, and if the work region is more homogeneous.

The biomass maps derived by the three methods (Inventory Polygons, Direct Radiometric Relationships and Regression-Kriging) for the whole study area are presented in Figure 7.

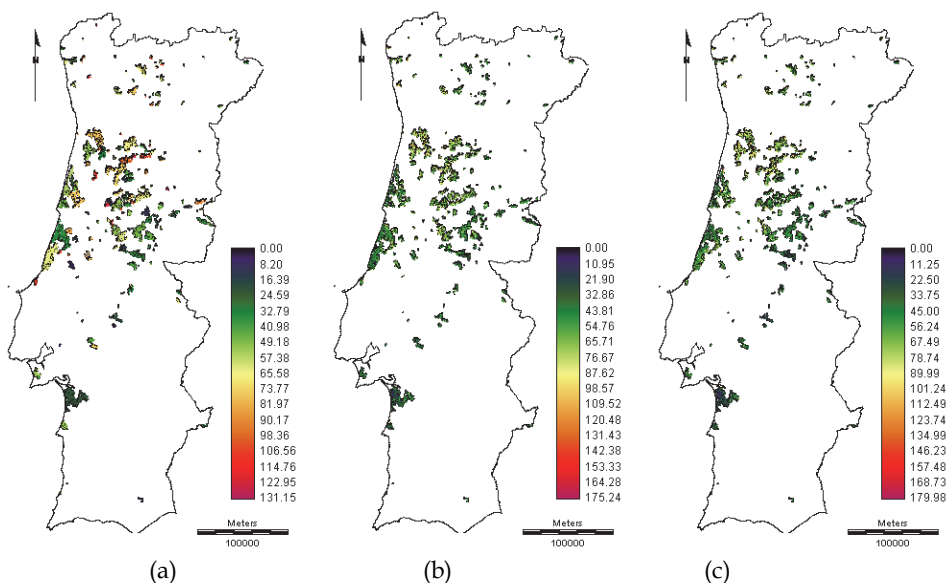


Fig. 7. Aboveground biomass maps (a) *Inventory Polygons* (b) *DRR* and (c) *RK*

### 3. Case study II – Biomass growth (NPP) of *Pinus pinaster* and *Eucalyptus globulus* stands, in the north of Portugal. Estimations by means of LANDSAT ETM+ images

#### 3.1 Study area

This research took place within an area in the northern part of Portugal where *Pinus pinaster* Ait. and *Eucalyptus globulus* Labill constitute the two most important forest species in terms of forested area (Figure 8).

The *P. pinaster* study area is a 60 km<sup>2</sup> rectangle (10 km × 6 km) with extensive stands of this species located at the north of Vila Real (41°39'N, 7°35'W) and the *E. globulus* study area is a 24km<sup>2</sup> rectangle (4 km × 6 km) of extensive stands of this species located at west of Vila Real (41°2'N, 7°43'W).

Both species are ecologically well adapted, despite *E. globulus* being an exotic tree, and the case study areas are representative of these ecosystems in Portugal. The *P. pinaster* forest is very heterogeneous in canopy density, has experienced only limited human intervention, and covers a wide range of structures, varying widely in terms of number of trees per hectare, average dimensions, and age groups. The *E. globulus* forest is much more homogeneous and has been more extensively investigated to enable greater timber production, which is very valuable for pulp production.

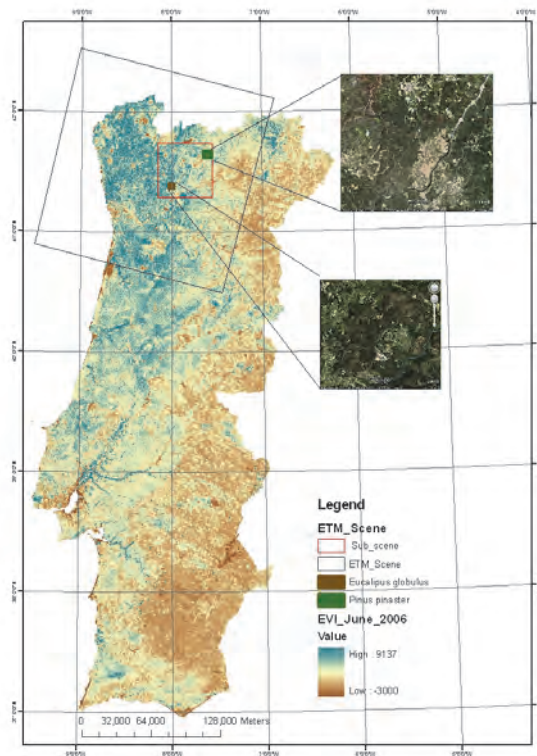


Fig. 8. Study area.

## 3.2 Methods and data

### 3.2.1 Methodology used in geometric and radiometric corrections

The available LANDSAT-7 ETM+ Image was acquired on the 15<sup>th</sup> of September 2001 at 10:02:13 (UTC). The image was geometrically and radiometrically corrected using MiraMon ("WorldWatcher"). This software allows displaying, consulting and editing raster and vector maps and was developed by the Autonomous University of Barcelona (UAB) remote sensing team. The software allows for the geometric correction of raster (e.g., IMG and JPG: satellite images, aerial photos, scan maps) or vector maps (e.g., VEC, PNT, ARC and POL and NOD), based on ground control points coordinates.

In the present research the ground control points were collected from Portuguese topographic maps on a 1/25000-scale, using the original ETM+ Scene. Twenty-five control points were collected (Toutin, 2004) to allow image correction and eleven control points were used for its validation. A first-degree polynomial correction was chosen for the geometric correction, using the nearest neighbour option for the resampling process.

Two Digital Elevation Models (DEMs) were constructed for each study area (*Pinus pinaster* and *Eucalyptus globulus* – see Figure 8), based on 10 m contour lines. The first DEM had a spatial resolution of 15 m and was used to correct the panchromatic band, mainly to allow identification of the ground control points due to its better spatial resolution. The second DEM had a spatial resolution of 20 m and was used for the correction of the LANDSAT ETM+ bands 1, 2, 3, 4, 5, and 7. Those 20 m DEMs were merged with a altitude model for Europe, with a pixel size of 1 Km. The radiometric correction was based on the lowest radiometric value for each band which is well known as the *kl*, and should be collected from the histogram analysis (Pons & Solé-Sugrañes, 1994 and Pons, 2002).

### 3.2.2 Methodology used to calculate vegetation indices

Within the study area, 31 sampling plots for the *Eucalyptus globulus* and 34 for the *Pinus pinaster* were surveyed and the coordinates of the centre of each plot recorded by Global Positioning System (GPS). The plots' location could then be identified on the geo-corrected images and reflectance data extracted for each ETM+ band. These data were then used to calculate a series of vegetation indices (Table 5), which were further used to analyse potential relationships with the forest variables.

In table 5, G represents the reflectance on the green wavelength; R is the reflectance in the red wavelength; NIR is the reflectance in the near infrared wavelength; and MIR1 and MIR2 are the reflectance in the two middle infrared bands from LANDSAT ETM+ image.

### 3.2.3 Model adjustment and selection

The available data (31 sampling plots for the *Eucalyptus globulus* and 34 for the *Pinus pinaster*) were divided in two groups, one for the adjustment of mathematical models and the other for the validation. An overall analysis of the correlation matrix allowed to identify the variables strongest related to NPP, which were then selected to establish regression models to Estimate NPP. The best NPP prediction models were selected based in the following statistics: the coefficient of determination ( $R^2$ ); the adjusted coefficient of determination ( $R^2_{adj}$ ); the root mean square error (RMSE); and the percentage root mean square error (RMSE%).

|   | Designation | Mathematical expression                | Source  |
|---|-------------|--|---|
| 1 | NDI(MIR1)   | $\frac{(NIR - MIR1)}{(NIR + MIR1)}$    | Lucas (1995)  |
| 2 | NDI(MIR2)   | $\frac{(NIR - MIR2)}{(NIR + MIR2)}$    | Lucas (1995)  |
| 3 | NDVI        | $\frac{(NIR - R)}{(NIR + R)}$          | Rouse <i>et al.</i> (1974); Bouman (1992); Malthus <i>et al.</i> (1993); Xia (1994); Nemani <i>et al.</i> (1993); Baret <i>et al.</i> (1995); Hamar <i>et al.</i> (1996); Fassnacht <i>et al.</i> (1997); Purevdorj <i>et al.</i> (1998); Todd <i>et al.</i> (1998); and Singh <i>et al.</i> (2003) |
| 4 | MVI1        | $\frac{MIR1}{MIR2}$                    | Fassnacht <i>et al.</i> (1997)  |
| 5 | MVI2        | $\frac{NIR}{MIR2}$                     | Fassnacht <i>et al.</i> (1997)  |
| 6 | RVI1        | $\frac{NIR}{R}$                        | Tucker (1979); Xia (1994); Baret <i>et al.</i> (1995); Hamar <i>et al.</i> (1996); Fassnacht <i>et al.</i> (1997); and Xu <i>et al.</i> (2003).   |
| 7 | TVI1        | $\sqrt{\frac{NIR}{R}}$                 | Tucker (1979)   |
| 8 | TVI2        | $\frac{(NIR + R)}{(NIR - R)}$          | Tucker (1979)   |
| 9 | TVI9        | $\sqrt{\frac{(G - R)}{(G + R)} + 0,5}$ | Tucker (1979)   |

Table 5. Vegetation indices used in the research

### 3.2.4 Comparison of the NPP images

NPP images obtained from different methodologies were compared by the *Kappa* index of agreement. Kappa was adopted by the remote sensing community as a useful measure of classification accuracy Rossiter (2004). The *Kappa* coefficient (*K*) measures pairwise agreement among a set of coders making category judgments, thus correcting values for expected chance of agreement (Carletta, 1996).

The overall *kappa* statistic, defining the overall proportion of area correctly classified, or in agreement, is calculated by the mathematical expression defined by Eq. 9 (Stehman, 1997; Rossiter, 2004):

$$\hat{k} = \frac{\sum_{i=1}^k P_{ii} - \sum_{i=1}^k P_{i+} \cdot P_{+i}}{1 - \sum_{i=1}^k P_{i+} \cdot P_{+i}} \quad (9)$$

where:

k = number of land-cover categories

$\sum_{i=1}^k p_{ii}$  represents the overall proportion of area correctly classified

$\sum_{i=1}^k P_{i+} \cdot P_{+i}$  is the expected overall accuracy if there were chance agreement between reference and mapped data

According to Green (1997) when there is complete agreement between two maps  $K=1$ , and a kappa value of zero, the two maps are said to be unrelated.

Moss (2004) considers that when Kappa is less than 0.20 the strength of agreement between both images is poor; between 0.21 and 0.40 fair; between 0.41 and 0.60 moderate; between 0.61 and 0.80 good; higher than 0.81 very good. However, according to Green (1997), kappa lower than 0.40 indicates a low degree of agreement; between 0.40 and 0.75 a fair to good degree of agreement; and higher than 0.75 a high degree of agreement.

### 3.3 Results and discussion

#### 3.3.1 Identification of the best prediction variables

In order to identify whether if it was possible to directly or indirectly estimate NPP from the remote sensing data, the Vegetation Index better correlated with NPP was identified from the general correlation matrix and analysed. The most relevant results are summarised in Table 6.

|           | <i>Pinus</i> NPP | <i>Eucalyptus</i> NPP |
|-----------|------------------|-----------------------|
| DN_B      | -0.179           | -0.739                |
| DN_G      | -0.268           | -0.692                |
| DN_R      | -0.194           | -0.688                |
| DN_NIR    | 0.344            | -0.280                |
| DN_MIR1   | -0.078           | -0.605                |
| DN_MIR2   | -0.174           | -0.614                |
| TVI2      | -0.142           | -0.535                |
| TVI9      | 0.030            | 0.288                 |
| MVI1      | 0.486            | 0.427                 |
| MVI2      | 0.435            | 0.318                 |
| NDVI      | 0.280            | 0.519                 |
| NDI(MIR1) | 0.181            | 0.386                 |
| NDI(MIR2) | 0.232            | 0.466                 |

Table 6. Correlation between NPP and the reflectance from each individual band and some vegetation indices

As presented in Table 6, *Pinus* NPP shows the higher correlation (positive) with the near infrared wavelength band, while *Eucalyptus* NPP is better correlated (negatively) with the middle infrared wavelength band.

The NDVI and TVI2 are the best correlated indices for the *Eucalyptus* and the MVI1 and MVI2 for the *Pinus*. These results reflect the initial observation when only reflectance from each individual band was analysed.

The best correlated vegetation indices were selected as independent variables for adjusting regression models to estimate NPP.

### 3.3.2 Models for the NPP *Eucalyptus globulus* estimation

The best mathematical models to estimate the NPP for the *Eucalyptus* stands and the basic statistics (ME and MAE) calculated from the validation dataset are presented in Table 7.

| Mathematical models   | NPP adjusted models statistics |                                |                 |                     | Validation dataset statistics |                |
|---|--------------------------------|--------------------------------|-----------------|---------------------|-------------------------------|----------------|
|   | R <sup>2</sup>                 | R <sup>2</sup> <sub>adj.</sub> | S <sub>yx</sub> | S <sub>yx</sub> (%) | ME                            | MAE            |
| $NPP=27.644-0.243B-0.0007GR^2-0.00014R^2$   | 0.613                          | 0.558                          | 2.988           | 22.5                | -1.631                        | 2.758          |
| $NPP_{arborescens}=89.260NDVI^2-117.195NDVI^3$<br>$NPP=-13.114+12.271NPP_{arborescens}-$<br>$1.818(NPP_{arborescens})^2+0.091(NPP_{arborescens})^3$ | 0.936<br>0.694                 | 0.933<br>0.695                 | 1.654<br>2.656  | 35.4                | 0.116<br>-1.198               | 1.238<br>3.098 |
| $NPP=3.593+167.750NDVI^2-233.667NDVI^3$   | 0.493                          | 0.447                          | 3.342           | 25.2                | -0.340                        | 2.959          |
| $NPP_{litter}=56.584NDVI^2-69.233NDVI^3$<br>$NPP=7.893(NPP_{litter})^{0.412}$   | 0.812<br>0.678                 | 0.805<br>0.666                 | 2.088<br>2.484  | 53.0<br>18.7        | -0.150<br>-0.589              | 1.309<br>2.834 |
| $NPP=17.672-0.611TVI2^2+0.048TVI2^3$  | 0.422                          | 0.370                          | 3.567           | 26.9                | -0.347                        | 2.903          |
| $G=13.431-155.484NDVI+648.846NDVI^2-$<br>$635.713NDVI^3$<br>$NPP=-5.787+4.652G-0.339G^2+0.008G^3$   | 0.657<br>0.634                 | 0.608<br>0.581                 | 4.170<br>2.908  | 33.1<br>21.6        | 1.121<br>-0.779               | 2.687<br>3.347 |
| $G=38.150-0.300GR-0.174MIR1$<br>$NPP=-5.787+4.652G-0.339G^2+0.008G^3$   | 0.793<br>0.634                 | 0.774<br>0.581                 | 3.168<br>2.908  | 33.7<br>21.6        | -1.754<br>-2.199              | 2.754<br>3.662 |

Table 7. Selected models to estimate *Eucalyptus* NPP, and validation dataset statistics

The observed standard error of the estimates are lower in the model using as independent variable the blue, the green and the red reflectances, and in the model using the NDVI, respectively. However, the model with NDVI as independent variable reveals a lower ME. Additionally, this model has a superior applicability since the individual bands reflectance have a great variation along the year, thus varying from image to image.

Based in the field measurements and in the estimated NPP, by the model using only the NDVI directly as independent variable ( $R^2=0.493$ ), two images were created for the entire study area (Figures 9a and 9b).

After the classification into four classes (1 -  $NPP < 5 \text{ ton ha}^{-1}\text{year}^{-1}$ ; 2 -  $5 \leq NPP < 10 \text{ ton ha}^{-1}\text{year}^{-1}$ ; 3 -  $10 \leq NPP < 15 \text{ ton ha}^{-1}\text{year}^{-1}$ ; and 4 -  $NPP > 15 \text{ ton ha}^{-1}\text{year}^{-1}$ ) the cross tabulation was carried out and the matrix error table analysed.

Kappa statistic showed a slight agreement around 37%. However, for a first approach these results are a good indicator for further studies. From the analyses of the *Eucalyptus* NPP map, obtained from fieldwork, it can be observed that there are no areas with an NPP lower than  $5 \text{ ton ha}^{-1}\text{year}^{-1}$ , and almost the whole *Eucalyptus* stand presents NPP figures between 10 and  $15 \text{ ton ha}^{-1}\text{year}^{-1}$ .

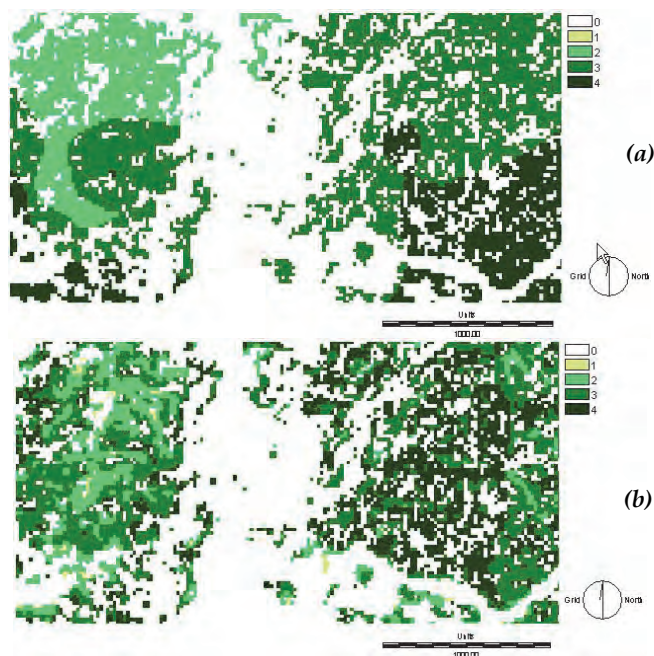


Fig. 9. *Eucalyptus* NPP estimations from field measurements (a) and NDVI model (b).

A significant result to estimate *Eucalyptus* NPP was obtained with the basal area (G) as independent variable ( $R^2=0.634$ ). In this case, the basal area can be estimated with acceptable confidence, using the NDVI or MIR1 as independent variables ( $R^2=0.657$  and  $0.793$ , respectively). In alternative, *Eucalyptus* NPP can also be estimated indirectly, with acceptable accuracies, by the litter present in the *Eucalyptus* stands ( $R^2=0.678$ ). A strong relationship was found between NPP from litter and NDVI ( $R^2=0.812$ ). The same methodology can be used by estimating, in a previous stage, the NPP arboreal with the NDVI as independent variable ( $R^2=0.936$ ) and subsequently, indirectly estimate the *Eucalyptus* NPP ( $R^2=0.694$ ).

### 3.3.3 Models for the NPP *Pinus pinaster* estimation

The best mathematical models to estimate the NPP for the *Pinus* stands and the basic statistics (ME and MAE) calculated from the validation dataset are presented in Table 8. The observed standard error of the estimates, as well the ME achieved from the validation dataset shows that the best model is obtained in the model using as independent variable the MVI1 for estimate the NPP of shrubs. The NPP of pine is subsequently estimated indirectly using this variable.

As in the *Eucalyptus* predictions the same methodology was implemented to compare the final maps achieved for the *Pinus* stands. The *Pine* NPP model using only the MVI1 as independent variable was used ( $R^2=0.417$ ). The two created maps for the entire study area (Figures 10a and 10b), were classified into four classes (1 -  $NPP < 5 \text{ ton ha}^{-1}\text{year}^{-1}$ ; 2 -  $5 \leq NPP < 10 \text{ ton ha}^{-1}\text{year}^{-1}$ ; 3 -  $10 \leq NPP < 15 \text{ ton ha}^{-1}\text{year}^{-1}$ ; and 4 -  $NPP > 15 \text{ ton ha}^{-1}\text{year}^{-1}$ ), a cross tabulation was carried out and the matrix error table analysed. Kappa statistic showed an

agreement around 48%, slightly better than in *Eucalyptus* estimations. However, it was observed that the achieved model was not able to identify and locate the extreme values of NPP (e.g. neither the most productive areas nor the least productive ones).

| Mathematical models                     | NPP adjusted models statistics |                                |                 |                     | Validation dataset statistics |       |
|---|--------------------------------|--------------------------------|-----------------|---------------------|-------------------------------|-------|
|   | R <sup>2</sup>                 | R <sup>2</sup> <sub>adj.</sub> | s <sub>yx</sub> | s <sub>yx</sub> (%) | ME                            | MAE   |
| $NPP=51.288-32.080MVI1+6.787MVI1^2$     | 0.417                          | 0.369                          | 4.617           | 31.7                | -0.902                        | 1.974 |
| $NPP_{shrubs}=-0.516MVI1^2+0.414MVI1^3$ | 0.816                          | 0.809                          | 2.614           | 71.3                | -0.279                        | 2.146 |
| $NPP=10.629+1.071NPP_{shrubs}$          | 0.649                          | 0.635                          | 3.508           | 27.5                | -0.317                        | 1.677 |
| $NPP_{shrubs}=1.146+0.142MVI1^2$        | 0.486                          | 0.466                          | 3.196           | 83.8                | -0.490                        | 2.268 |
| $NPP=10.629+1.071NPP_{shrubs}$          | 0.649                          | 0.635                          | 3.508           | 27.6                | -0.842                        | 2.276 |

Table 8. Selected models to estimate *Pinus* NPP and validation dataset statistics

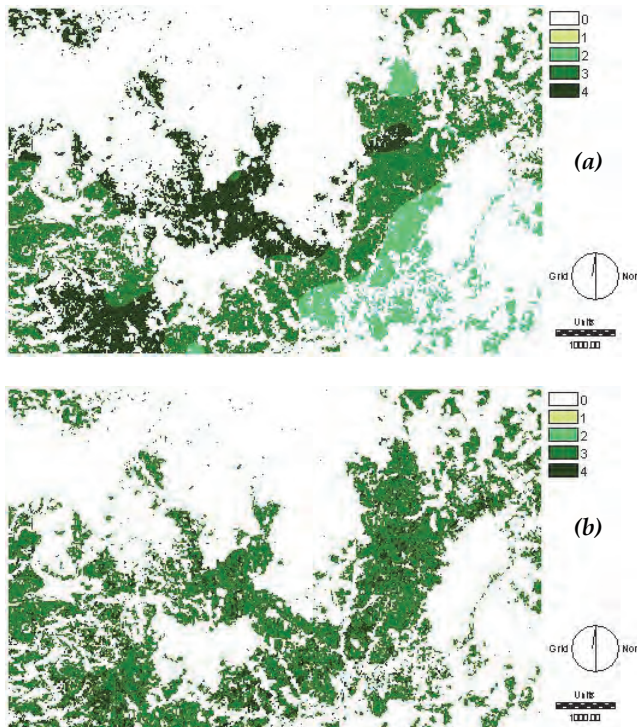


Fig. 10. *Pinus* NPP estimations from field measurements (a), and the MVI1 model (b).

For the *Pinus* stands, it was possible to estimate the total NPP ( $R^2=0.816$ ) knowing only the NPP from shrubs. In this case, the NPP from shrubs was predicted using the MVI as auxiliary variable ( $R^2=0.645$ ).

## 4. Conclusions

In this research, AGB and NPP estimates were carried out by means of forest inventory data remote sensing imagery and geostatistical modeling. The general conclusions are:

In the case study I, tree Aboveground biomass (AGB) mapping approaches were compared: Inventory Polygons; Direct Radiometric Relationships (DRR) and Regression-kriging (RK). Pure pine stands were mapped and AGB estimates were achieved using data collected in the National Forest inventory dataset. The Inventory polygons method was used since the field plots of forest inventory dataset fall within all the polygons of the forest cover map. At the same time, this approach was used to compare and validate DRR and RK methods.

The results showed that DRR and RK, using Vegetation Indices transformed from MODIS remotely sensed data, can be used for biomass mapping purposes. However, it should be pointed out that, in the present research, the coarse resolution of MODIS (250m) data associated with small polygons of the pine landcover class did not allow to extract the pure spectral response of this vegetation type. Hence, the correlation between AGB and NDVI as independent variable is not as high as desired.

This limitation can be overcome by using images with higher spatial resolution. Moreover, these methodologies can be applied with greater accuracy in areas where land cover polygons are large enough to minimize, as much as possible, the effect of edging.

The analysis of statistical parameters of validation dataset such as the mean error (ME), the mean absolute error (MAE), standard deviation (SD) and the root mean squared error (RMSE) show that RK, making use of geostatistical modeling techniques, combined with remote sensing data as auxiliary variable improves the predictions when compared to DRR. Furthermore, RK has the advantage of generating estimates for the spatial distribution of AGB and its uncertainty for the study area. The uncertainty maps allow the evaluation of the reliability of estimates by identifying the sites with major uncertainties which can be useful to select different estimation methods for those areas.

In the case study II, some simplified methodologies were proposed to estimate NPP. For the *Eucalyptus* ecosystem using the basal area or the NPP from litter, and for the *Pinus* ecosystem using the NPP from shrubs.

Despite the direct NPP estimation from remote sensing data did not provide very promising results, it was possible to establish indirect relationships between some vegetations indices calculated from Landsat ETM+ imagery data and the litter NPP, shrubs NPP and from basal area of the studied forest stands.

Those simplifications can be extremely important when time and economic resources are limited. The importance of those methodologies could become more relevant as NPP is a variable very difficult to obtain, consuming time and demanding hard fieldwork.

The loss in accuracy is certainly compensated by decrease of fieldwork. The balance between both should only be taken in each particular case, considering the general context of each situation (e.g., time and funds available, human resources available, objectives of the research).

## 5. Acknowledgements

Authors would like to express their acknowledgement to the Portuguese Science and Technology Foundation (FCT), programmes SFRH/PROTEC/49626/2009 and FCT FCOMP-01-0124-FEDER-007010 (PTDC/AGR-CFL/68186/2006).

## 6. References

- AFN (2006). Dados do Inventário Florestal Nacional (05/06) Information retrieval tool. Autoridade Florestal Nacional. Ministério da Agricultura do Desenvolvimento Rural e das Pescas, Lisboa.
- Ahmed, S., & de Marsily, G (1987). Comparison of geostatistical methods for estimating transmissivity using data on transmissivity and specific capacity. *Water Resources Research* 23(9): 1717-1737.
- Atkinson, P. M.; Foody, G. M.; Curran, P. J., & Boyd D. S. (2000). Assessing the ground data requirements for regional scale remote sensing of tropical forest biophysical properties. *International Journal of Remote Sensing* 21(13-14): 2571-2587.
- Baret, F., Clevers, J.G. and Steven, M.D. (1995). The robustness of canopy gap fraction estimates from red and near-infrared reflectances: A comparison of approaches. *Remote Sensing of Environment* 54: 141-151.
- Bouman, B.M. (1992). Accuracy of estimating the leaf area index from vegetation indices derived from crop reflectance characteristics: a simulation study. *International Journal of Remote Sensing* 13(16): 3069-3084.
- Burcsu, T. K., Robeson, S. M., & Meretsky, V.J. (2001). Identifying the Distance of Vegetative Edge Effects Using Landsat TM Data and Geostatistical Methods. *Geocarto International* 16( 4): 61-70.
- Cao, M. and Woodward, F.I. (1998). Net primary and ecosystem production and carbon stocks of terrestrial ecosystems and their responses to climate change. *Global Change Biology* 4: 185-198.
- Carletta, J. (1996). Assessing agreement on classification tasks: the kappa statistic. *Computational linguistics* 22(2): 1-6.
- Chirici, Gherardo; Barbati, Anna, & Maselli, Fabio (2007). Modelling of Italian forest net primary productivity by the integration of remotely sensed and GIS data. *Forest Ecology and Management* 246: 285-295.
- Cressie, N. A. C. (1993). *Statistics for Spatial Data*. New York, USA: John Wiley & Sons. pp. 416.
- Curran, P.J. (1988). The semivariogram in remote sensing: An introduction. *Remote Sensing of Environment* 24: 493-507.
- Deutsch, C. V., & Journel A. G. (1998). *Geostatistical Software Library and User's Guide*. (2nd ed.). New York, USA: Oxford University Press, pp. 369.
- Eastman, J. R. (2006). *Idrisi Andes. Guide to GIS and Image Processing*. USA: Clark Labs. Clark University, pp. 328.
- Fassnacht, K.S., Gower, S.T., MacKenzie, M.D., Nordheim, E.V. and Lillesand, T.M. (1997). Estimating the leaf area index of north central Wisconsin forests using the Landsat Thematic Mapper. *Remote Sensing of Environment* 61: 229-245.
- Field, C.B., Randerson, J.T. and Malmstrom, C.M. (1995). Global net primary production: combining ecology and remote sensing. *Remote Sensing of Environment* 51: 74-88.
- García-Martín, A., Pérez-Cabello, F., de la Riva, J. R., & Montorio, R. (2008). Estimation of crown biomass of Pinus spp. from Landsat TM and its effect on burn severity in a Spanish fire scar. *IEEE Journal of Selected Topics in Applied Earth Observations and Remote Sensing* 1(4): 254-265.
- Goovaerts, P. (1997). *Geostatistics for Natural Resources Evaluation*. New York, USA: Oxford University Press, Inc., pp. 496.

- Goovaerts, P. (1999). Using elevation to aid the geostatistical mapping of rainfall erosivity. *Catena* 34(3-4): 227-242.
- Green, A.M. (1997). Kappa statistics for multiple raters using categorical classifications, *Proceedings of the twenty-second annual SAS @Users Group International Conference*, Cary, NC: SAS Institute, Inc: 1110-1115.
- Hamar, D., Ferencz, C., Lichtenberger, J., Tarcsa, G. and Ferencz-Árkos, I. (1996). Yield estimation for corn and wheat in the hungarian great plain using landsat MSS data. *International Journal of Remote Sensing* 17(9): 1689-1699.
- Häme, T., Salli, A., Andersson, K., & Lohi, A. (1997). A new methodology for estimation of biomass of conifer-dominated boreal forest using NOAA AVHRR data. *International Journal of Remote Sensing* 18: 3211-3243.
- Hengl T., Heuvelink G. M. B., & Stein A. (2004). A generic framework for spatial prediction of soil variables based on regression-kriging. *Geoderma* 122(1-2): 75-93.
- Hengl T., Heuvelink, G. B. M. & Rossiter, D. G. (2007). About regression-kriging: from equations to case studies. *Computers and Geosciences* 33(10): 1301-1315.
- Hengl, T. (2009). *A Practical Guide to Geostatistical Mapping*. Amsterdam, ISBN 978-90-9024981-0.
- Hese, S., Lucht, W., Schmulilius, C., Barnsley, M., Dubayah, R., Knorr, D., Neumann, K., Riedel, T., & Schröter, K. (2005). Global biomass mapping for an improved understanding of the CO<sub>2</sub> balance-the Earth observation mission Carbon-3D. *Remote Sensing of Environment* 94(1): 94-104.
- Hu, Huifeng, & Wang, G. G. (2008). Changes in forest biomass carbon storage in the South Carolina Piedmont between 1936 and 2005. *Forest Ecology and Management* 255(5-6): 1400-1408.
- Hyde, P., Nelson, R., Kimes, D., & Levine, E. (2007). Exploring LiDAR-RaDAR synergy-predicting aboveground biomass in a southwestern ponderosa pine forest using LiDAR, SAR and InSAR. *Remote Sensing of Environment* 106(1): 28-38.
- IGP (2010). *CLC2006 – Cartografia CORINE Land Cover 2006 para Portugal Continental; 2009*. <<http://www.igeo.pt/gdr/projectos/clc2006/>> (verified 01.01.2010).
- Isaaks, E. H., & Srivastava, R. M. (1989). *An Introduction to Applied Geostatistics*. New York, USA: Oxford University Press, pp. 542.
- Jarlan, L., Mangiarotti, S., Mougín E., Mazzega, P., Hiernaux, P., & Le Dantec, V. (2008). Assimilation of SPOT/VEGETATION NDVI data into a sahelian vegetation dynamics model. *Remote Sensing of Environment* 112(4): 1381-1394.
- Knotters, M., Brus, D. J., & Voshaar, J. H. O. (1995). A comparison of kriging, co-kriging and kriging combined with regression for spatial interpolation of horizon depth with censored observations. *Geoderma* 67(3-4): 227-246.
- Labrecque, S., Fournier, R. A., Luther, J. E., & Piercey, D. (2006). A comparison of four methods to map biomass from Landsat-TM and inventory data in western Newfoundland. *Forest Ecology and Management* 226, 129-144.
- Liao, J., Dong, L., & Shen, G. (2009). Neural network algorithm and backscattering model for biomass estimation of wetland vegetation in Poyang Lake area using Envisat ASAR data. *Geoscience and Remote Sensing Symposium, IEEE International, IGARSS 2009*.
- Lloyd, C. D. (2007). *Local Models for Spatial Analysis*. Boca Raton: CRC Press, Taylor & Francis Group.

- Lu, D. (2006). The potential and challenge of remote sensing-based biomass estimation. *International Journal of Remote Sensing* 27: 1297-1328.
- Lucas, N.S. (1995). *Coupling remotely sensed data to a forest ecosystem simulation model*. Thesis for the Degree of Doctor of Philosophy, University of Wales, Swansea, England, pp. 375.
- Madugundu, R.; Nizalapur, V. & Jha, C. S. (2008). Estimation of LAI and above-ground biomass in deciduous forests: Western Ghats of Karnataka, India. *International Journal of Applied Earth Observation and Geoinformation* 10(2): 211-219.
- Malthus, T.J., Andrieu, B., Danson, F.M., Jaggard, K.W. and Steven, M.D. (1993). Candidate high spectral resolution infrared indices for crop cover. *Remote Sensing of Environment* 46: 204-212.
- Matheron G. (1963). Principles of geostatistics. *Economic Geology* 58: 1246-1266.
- Matheron G. (1971). *The theory of regionalised variables and its applications*. Les Cahiers du Centre de Morphologie Mathématique de Fontainebleau. Paris: Ecole Nationale Supérieure de Paris, pp. 212.
- Melillo, J.M., McGuire, A.D., Kicklighter, D.W., Moore III, B., Vorosmarty, C.J. and Schloss, A.L. (1993). Global climate change and terrestrial net primary production. *Nature* 363: 234-240.
- Meng, Q., Cieszewski, C. J., Madden, M., & Borders, B. E. (2007). K Nearest Neighbor method for forest inventory using remote sensing data. *GIScience & Remote Sensing* 44(2): 149-165.
- Meng, Q.; Cieszewski, C. J. & Madden, M. (2009). Large area forest inventory using Landsat ETM+: A geostatistical approach. *ISPRS Journal of Photogrammetry and Remote Sensing* 64: 27-36.
- Moss, S. (2004). Kappa statistics. The Institute of Cancer Research, [http://www.icr.ac.uk/cseu/bc\\_eqa\\_kappa.html](http://www.icr.ac.uk/cseu/bc_eqa_kappa.html).
- Muukkonen, P., & Heiskanen, J. (2007). Biomass estimation over a large area based on standwise forest inventory data and ASTER and MODIS satellite data: A possibility to verify carbon inventories. *Remote Sensing of Environment* 107: 617-624.
- Nemani, R., Pierce, L., Running, S. and Band, L. (1993). Forest ecosystem processes at the watershed scale: sensitivity to remotely-sensed leaf area index estimates. *International Journal of Remote Sensing* 14(13): 2519-2534.
- Odeh, I. O. A., McBratney, A. B., & Chittleborough, D. J. (1994). Spatial prediction of soil properties from landform attributes derived from a digital elevation model. *Geoderma*, 63: 197-214.
- Odeh, I.O. A., McBratney, A. B., & Chittleborough, D. J. (1995). Further results on prediction of soil properties from terrain attributes: heterotopic cokriging and regression-kriging. *Geoderma* 67(3-4): 215-226.
- Palmer, D. J.; Höck, B. K.; Kimberley, M. O.; Watt, M. S.; Lowe, D. J. & Payn, T. W. (2009). Comparison of spatial prediction techniques for developing Pinus radiata productivity surfaces across New Zealand. *Forest Ecology and Management* 258: 2046-2055.
- Pebesma, E. (2001). *Gstat user's manual*. University of Utrecht, pp. 108.
- Pebesma, E. (2004). Multivariable geostatistics in S: the gstat package. *Computers & Geosciences* 30(7): 683-691.

- Pons, X and Solé-Sugrañes, L. (1994). A simple radiometric correction model to improve automatic mapping of vegetation from multispectral satellite data. *Remote Sensing of Environment* 48: 191-204.
- Pons, X. (2002). *MiraMon. Geographic information system and remote sensing software* Centre de Recerca Ecològica i Aplicacions Forestals, CREAM. Bellaterra. ISBN: 84-931323-5-7.
- Purevdorj, T., Tateishi, R., Ishiyamas, T., and Honda, Y. (1998). Relationships between percent cover and vegetation indices. *International Journal of Remote Sensing* 19(18): 3519-3535.
- Rahman, M. M.; Csaplovics, E., & Koch, B. (2005). An efficient regression strategy for extracting forest biomass information from satellite sensor data. *International Journal of Remote Sensing* 26(7): 1511-1519.
- Rossiter, D.G. (2004). *Statistical method for accuracy assessment of classified thematic map*. International Institute for Geo-information Science and Earth, Department of Earth Systems Analysis, Enschede, NL, pp. 46.
- Rouse, J.W., Haas, R.H., Schell, J.A., Deering, D.W. and Harlan, J.C. (1974). *Monitoring the vernal advancement retrogradation of natural vegetation*. Final Report Type III, NASA/GSFC, Greenbelt, MD., USA, pp. 371.
- Sales, M. H., Souza Jr., C. M., Kyriakidis, P. C.; Roberts, D. A., & Vidal, E. (2007). Improving spatial distribution estimation of forest biomass with geostatistics: A case study for Rondônia, Brazil. *Ecological Modelling* 205: 221-230.
- Sen, Zekai (2009). *Spatial Modeling Principles in Earth Sciences*. London, New York: Springer Dordrecht Heidelberg, pp. 351.
- Singh, R.P., Roy, S., and Koogan, F. (2003). Vegetation and temperature condition indices from NOAA AVHRR data for drought monitoring over India. *International Journal of Remote Sensing* 24 (22): 4393-4402.
- Stehman, S.V. (1997). Selecting and interpreting measures of thematic classification accuracy. *Remote Sensing of Environment* 62: 77-89.
- Todd, S.W., Hoffer, R.M., and Milchunas, D.G. (1998). Biomass estimation on grazed and ungrazed rangelands using spectral indices. *International Journal of Remote Sensing* 19 (3): 427-438.
- Tomppo, E. (1991). Satellite imagery-based national inventory of Finland. *International Archives of Photogrammetry and Remote Sensing* 28(7-1): 419-424.
- Tomppo, E., Nilsson, M., Rosengren, M., Aalto, P., Kennedy, P. (2002). Simultaneous use of Landsat-TM and IRS-1c WiFS data in estimating large area tree stem volume and aboveground biomass. *Remote Sensing of Environment* 82: 156-171.
- Toutin, T. (2004). Review article: Geometric processing of remote sensing images: models, algorithms and methods. *International Journal of Remote Sensing* 25(10): 1893-1924.
- Tucker, C.J. (1979). Red and photographic infrared linear combinations for monitoring vegetation. *Remote Sensing of Environment* 8: 127-150.
- Waring, R.H., Landsberg, J.J. and Williams, M. (1998). Net primary production of forests: a constant fraction of gross primary production? *Tree Physiology* 18: 129-134.
- Webster, R. & Oliver, M. A. (1992). Sample adequately to estimate variograms of soil properties. *Journal of Soil Science* 43: 177-192.
- Webster, R. & Oliver, M. A. (2007). *Geostatistics for Environmental Scientists*. (2nd ed.), England: John Wiley & Sons Ltd, pp.332.

- Woodcock, C. E, Strahler, A. H., & Jupp, D. L. B. (1988). The use of variograms in remote sensing: II. Real digital images. *Remote Sensing of Environment* 25: 349-379.
- Xia, L., 1994. A two-axis adjusted vegetation index (TWVI). *International Journal of Remote Sensing* 15(7): 1447-1458.
- Xu, B., Gong, P., and Pu, R. (2003). Crown closure estimation of oak savannah in a dry season with Landsat TM imagery: comparison of various indices through correlation analysis. *International Journal of Remote Sensing* 24 (9): 1811-1822.
- Zheng, D., Heath, L. S., & Ducey, M. J. (2007). Forest biomass estimated from MODIS and FIA data in the Lake States: MN, WI and MI, USA. *Forestry* 80(3): 265-278.